Solution Structure of ZipA, a Crucial Component of *Escherichia coli* Cell Division†

Franklin J. Moy,§ Elizabeth Glasfeld,‡ Lidia Mosyak,§ and Robert Powers*,§

Department of Biological Chemistry, Wyeth Research, 85 Bolton Street, Cambridge, Massachusetts 02140, and Department of Infectious Disease, Wyeth Research, 401 North Middletown Road, Pearl River, New York 10965

Received April 27, 2000; Revised Manuscript Received May 30, 2000

ABSTRACT: ZipA, an essential component of cell division in *Escherichia coli*, interacts with the FtsZ protein at the midcell in one of the initial steps of septum formation. The high-resolution solution structure of the 144-residue C-terminal domain of *E. coli* ZipA ($ZipA_{185-328}$) has been determined by multidimensional heteronuclear NMR. A total of 30 structures were calculated by means of hybrid distance geometry-simulated annealing using a total of 2758 experimental NMR restraints. The atomic root means square distribution about the mean coordinate positions for residues 6−142 for the 30 structures is 0.37 ± 0.04 Å for the backbone atoms, 0.78 ± 0.05 Å for all atoms, and 0.45 ± 0.04 Å for all atoms excluding disordered side chains. The NMR solution structure of $ZipA_{185-328}$ is composed of three α-helices and a β-sheet consisting of six antiparallel β-strands where the α-helices and the β-sheet form surfaces directly opposite each other. A C-terminal peptide from FtsZ has been shown to bind $ZipA_{185-328}$ in a hydrophobic channel formed by the β-sheet providing insight into the ZipA−FtsZ interaction. An unexpected similarity between the $ZipA_{185-328}$ fold and the split β−α−β fold observed in many RNA binding proteins may further our understanding of the critical ZipA−FtsZ interaction.

Bacterial cell division is a complex series of events in which a common feature is the formation of a septum across the middle of the cell (for reviews see refs *1*−*3*). In *Escherichia coli*, at least nine essential components are involved in the assembly of the septal ring, a membrane-associated cytoskeletal element that directs the formation of the septum. FtsZ is a major component of the septal ring and a highly ubiquitous and abundant protein conserved among most bacterial cells. During the initial stage of cell division, FtsZ moves from the cytoplasm to accumulate at the division site where it self-assembles into a ring-like polymer structure associated with the inner surface of the cytoplasmic membrane. The resulting FtsZ ring provides a scaffold to recruit other members of the septal ring. ZipA is one of the first proteins recruited to the division site and has been shown to directly bind FtsZ (*4*−*6*).

ZipA is essential for cell division and viability in *E. coli* (*4*). Experiments with the green fluorescent protein fusion of ZipA have demonstrated that only prior localization of FtsZ is required for localization of ZipA to midcell (*5*, *6*). Changes in the relative abundance of ZipA in the cell, either by depletion or overexpression, result in filamentation. The morphology of these filaments resembles those observed for cells in which FtsZ has been depleted. This is consistent with the observation that both ZipA and FtsZ are involved at the very early stage of cell division.

ZipA is a 328-amino acid protein that is composed of five regions or domains (*4*). The N-terminus is a highly hydrophobic region of approximately 25 amino acids which form the transmembrane domain that anchors the protein to the cytoplasmic membrane. This is followed by a basic region (∼23 aa), an acidic region (∼17 aa), and a long proline rich region (residues 86−188). The C-terminal domain (residues 189−328) has been shown to be sufficient for binding to FtsZ (*6*) and has several areas that are conserved among the seven ZipA sequences identified to date. Since ZipA is anchored to the cytoplasmic membrane while binding FtsZ, it has been speculated that the function of ZipA may be to link the membrane with the FtsZ rings, to stabilize or organize the FtsZ rings, or to link invagination of the membrane to constriction of the FtsZ ring during septation (*4*−*7*). Since changes in the relative abundance of ZipA in the cell result in filamentation, disruption of the ZipA−FtsZ interaction would likely disrupt cell division and cause cell lysis, suggesting that the ZipA−FtsZ interaction may be a viable therapeutic target for drug development. To better understand the role of ZipA in cell division and as part of a structure-based drug design program, we have determined the high-resolution solution structure of the C-terminal domain of ZipA ($ZipA_{185-328}$, where M185 corresponds to M1 in the NMR structure) by heteronuclear multidimensional NMR and have explored its interaction with FtsZ.

MATERIALS AND METHODS

NMR Sample Preparation. Uniformly (>95%) ^{15}N- and $^{15}N/^{13}C$-labeled recombinant $ZipA_{185-328}$ was expressed in *E. coli* and purified as described elsewhere (*8*). The NMR samples contained 1 mM of $ZipA_{185-328}$ in a buffer containing 50 mM sodium phosphate, 2 mM NaN_3, and 50 mM KCl,

† Atomic coordinates for the 30 final simulated annealing structures and the restrained minimized mean structure of $ZipA_{185-328}$ have been deposited in the Protein Data Bank (PDB ID code 1F7X and 1F7W).

* To whom correspondence should be sent at Wyeth Research, 85 Bolton St., Rm 222B, Cambridge, MA 02140. Phone: (617) 665-7997. Fax: (617) 665−8993. E-mail: powersr@war.wyeth.com.

§ Department of Biological Chemistry.

‡ Department of Infectious Disease.

10.1021/bi0009690 CCC: $19.00 © 2000 American Chemical Society
Published on Web 07/07/2000

in either 90% H_2O/10% D_2O or 100% D_2O at pH 5.5. For the 2D ^1H-^{15}N HSQC chemical shift perturbation studies, the FtsZ C-terminal peptide, KEPDYLDIPAFLRKQAD, was in ~5-fold excess relative to a $ZipA_{185-328}$ concentration of 0.3 mM where buffer conditions were identical to above. For structural analysis of the ZipA complexed with the FtsZ C-terminal peptide, the peptide was in either a ~5-fold excess or equimolar relative to a $ZipA_{185-328}$ concentration of 1 mM where buffer conditions were identical as above.

NMR Data Collection. All NMR spectra were recorded at 25 °C on a Bruker DRX 600 spectrometer equipped with a triple-resonance gradient probe. For spectra recorded in H_2O, water suppression was achieved with the WATERGATE sequence and water-flip back pulses (*9*, *10*). Quadrature detection in the indirectly detected dimensions were recorded with States-TPPI hypercomplex phase increment (*11*). Spectra were collected with appropriate refocusing delays to allow for 0,0 or −90,180 phase correction. Spectra were processed using the NMRPipe software package (*12*) and analyzed with PIPP (*13*) on a Sun Ultra10 Workstation. When appropriate, data processing included a solvent filter, zero-padding data to a power of two, linear predicting back one data point of indirectly acquired data to obtain zero phase corrections and linear prediction of additional points for the indirectly acquired dimensions to increase resolution. Linear prediction by the means of the mirror image technique was used only for constant-time experiments (*14*). In all cases, data were processed with a skewed sine-bell apodization function, and one zero-filling was used in all dimensions.

^1H, ^{15}N, ^{13}C, and ^{13}CO assignments and secondary structure determination of $ZipA_{185-328}$ were reported previously (*8*). In addition to the NMR experiments used for the $ZipA_{185-328}$ resonance assignments, the present structure is based on the following series of spectra: HNHA (*15*), HNHB (*16*), HACAHB-COSY (*17*), 3D ^{15}N- (*18*, *19*), and ^{13}C-edited NOESY (*20*, *21*). The ^{15}N-edited NOESY and ^{13}C-edited NOESY experiments were collected with 100 and 120 ms mixing times, respectively.

The assignments of the ^1H, ^{15}N, and ^{13}C resonances of $ZipA_{185-328}$ in the complex with FtsZ C-terminal peptide were based on the assignments previously reported for free $ZipA_{185-328}$ (*8*) in combination with a minimal set of experiments obtained for the complex: 2D ^1H-^{15}N HSQC, 3D ^{15}N-edited NOESY (*18*, *19*), CBCA(CO)NH (*22*), C(CO)NH (*23*), HC(CO)NH (*23*), and HNHA (*15*) to assign regions of the $ZipA_{185-328}$ spectra perturbed by the presence of the FtsZ peptide. The resonance assignments for $ZipA_{185-328}$ in the complex followed the procedure described previously (*24*). The resonance assignments of the free FtsZ C-terminal peptide were based on 2D NOESY (*25*), 2D TOCSY (*26*), and 2D COSY (*27*) experiments. The assignments followed the protocol described by Wuthrich (*28*). The resonance assignments for the FtsZ C-terminal peptide in the complex with $ZipA_{185-328}$ were based on the free peptide assignments and the 2D $^{12}C/^{12}C$-filtered NOESY (*29*) and 3D ^{13}C-edited/^{12}C-filtered NOESY (*30*) spectra of the complex.

Analysis of the $ZipA_{185-328}$ complex with the FtsZ C-terminal peptide is based on observed NOEs from the 3D ^{13}C-edited/^{12}C-filtered NOESY (*30*) experiment. The 3D ^{13}C-edited/^{12}C-filtered NOESY experiment was collected with 110 and 300 ms mixing times. As a result of the weak binding affinity of the FtsZ C-terminal peptide ($K_d \approx 20$ μM) with $ZipA_{185-328}$ only a minimal number of intermolecular NOEs (36) were observed with a 5-fold excess of FtsZ C-terminal peptide relative to $ZipA_{185-328}$. The weak affinity of the peptide for $ZipA_{185-328}$ complicated both the observation of intramolecular NOEs and the assignment of the FtsZ C-terminal peptide NMR resonances in the presence of $ZipA_{185-328}$. When the FtsZ C-terminal peptide was in approximately 5-fold excess relative to $ZipA_{185-328}$, the 2D-filtered experiments yielded spectra consistent with the free peptide assignments. Conversely, when the FtsZ C-terminal peptide concentration was reduced to an equimolar amount relative to $ZipA_{185-328}$, resonances in the 2D-filtered experiments exhibited chemical shift perturbations relative to the free peptide but with a significant reduction in signal-to-noise prohibiting the observation of structurally relevant intramolecular NOEs. Further complicating the analysis of the 3D ^{13}C-edited/^{12}C-filtered NOESY experiment was the observation of NOEs from $ZipA_{185-328}$ to either free or bound FtsZ C-terminal peptide NMR resonances. Apparently, the affinity of the peptide for $ZipA_{185-328}$ varied along the binding site resulting in distinct off-rates for different regions of the peptide where some NOEs behaved effectively as transfer-NOEs. Therefore, the assignments of the intermolecular NOEs from the 3D ^{13}C-edited/^{12}C-filtered NOESY experiment were obtained by comparison of the data from the free and bound forms of the peptide where the aromatic residues were readily identified. Additionally, correct assignments were ascertained by consistency with the $ZipA_{185-328}$−FtsZ peptide complex.

Interproton Distance Restraints. The NOEs assigned from 3D ^{13}C-edited NOESY and 3D ^{15}N-edited NOESY experiments were classified into strong, medium, weak, and very weak corresponding to interproton distance restraints of 1.8−2.7 Å (1.8−2.9 Å for NOEs involving NH protons), 1.8−3.3 Å (1.8−3.5 Å for NOEs involving NH protons), 1.8−5.0 Å, and 3.0−6.0 Å, respectively (*31*, *32*). Upper distance limits for distances involving methyl protons and nonstereospecifically assigned methylene protons were corrected appropriately for center averaging (*33*).

Torsion Angle Restraints and Stereospecific Assignments. The β-methylene stereospecific assignments and χ_1 torsion angle restraints were obtained primarily from a qualitative estimate of the magnitude of $^3J_{\alpha\beta}$ coupling constants from the HACAHB-COSY experiment (*17*) and $^3J_{N\beta}$ coupling constants from the HNHB experiment (*16*). Val γ-methyl stereospecific assignments were made from the relative intensity of intraresidue NH−CγH and CαH−CγH NOEs (*34*). Leu and Ile χ_2 torsion angle restraints and Leu δ-methyl stereospecific assignments were obtained primarily from $^{13}C-^{13}C$-long-range coupling constants (*35*) and the relative intensity of intramolecular NOEs (*36*). Further support for the assignments was obtained from approximate distance restraints for intraresidue NOEs involving NH, CαH, and CβH protons (*36*).

The ϕ and ψ torsion angle restraints were obtained from $^3J_{NH\alpha}$ coupling constants measured from the HNHA experiment (*15*) and from chemical shift analysis using the TALOS program (*37*). The minimum ranges employed for the ϕ, ψ, and χ torsion angle restraints were ±30, ±50, and ±20°, respectively.

Initially, NOEs to degenerate CδH and CϵH resonances from Phe and Tyr residues use pseudo-atoms during the

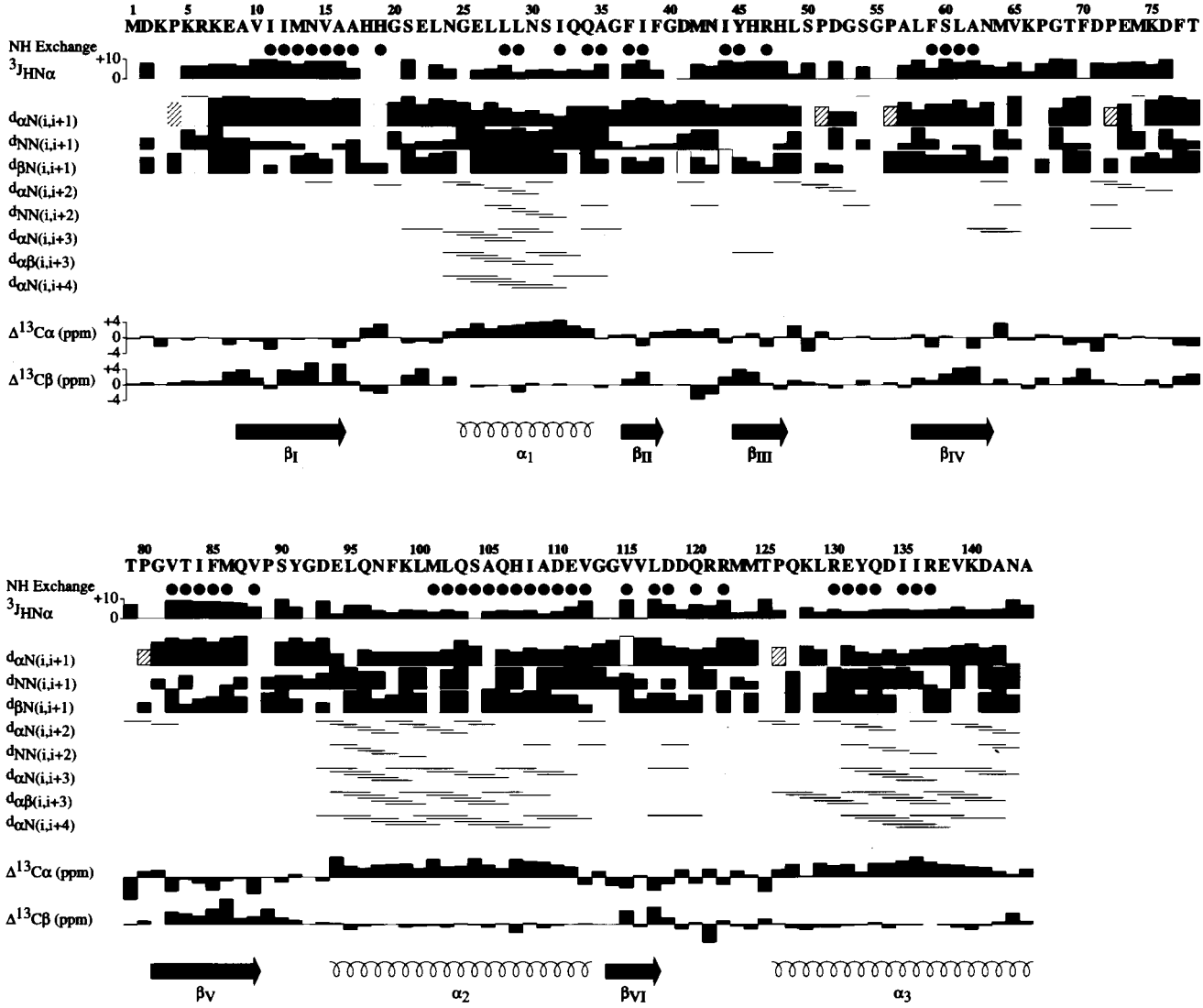

FIGURE 1: Summary of the sequential and medium range NOEs involving the NH, Hα, and H$\beta\beta$ protons, the amide exchange and $^3J_{HN\alpha}$ coupling constant data, and the $^{13}C\alpha$ and $^{13}C\beta$ secondary chemical shifts observed for RGS4 with the secondary structure deduced from these data. Thickness of the lines reflects the strength of the NOEs. Amide protons still present after exchange to D_2O are indicated by closed circles. Open boxes represent potential sequential assignments NOEs that are obscured by resonance overlap and could therefore not be assigned unambiguously. Hashed boxes on the same line as the Hα(i)-NH(i+1) NOEs represent the sequential NOE between the Hα proton of residue i and the CδH proton of the i + 1 proline and is indicative of a trans proline.

structure calculation. At later stages in the refinement when the quality of the $ZipA_{185-328}$ structure has significantly improved, it is possible to assign NOE distance restraints to CδH and CϵH of well-defined Phe and Tyr to only one side of the ring and assign a χ_2 torsion angle restraint.

Structure Calculations. The structures were calculated using the hybrid distance geometry-dynamical simulated annealing method of Nilges et al. (*38*) with minor modifications (*39*) using the program XPLOR (*40*), adapted to incorporate pseudopotentials for $^3J_{NH\alpha}$ coupling constants (*41*), secondary $^{13}C\alpha/^{13}C\beta$ chemical shift restraints (*42*), and a conformational database potential (*43*, *44*). The target function that is minimized during restrained minimization and simulated annealing comprises only quadratic harmonic terms for covalent geometry, $^3J_{NH\alpha}$ coupling constants and secondary $^{13}C\alpha/^{13}C\beta$ chemical shift restraints, square-well quadratic potentials for the experimental distance and torsion angle restraints, and a quartic van der Waals term for nonbonded contacts. All peptide bonds were constrained to be planar and trans except for cis prolines P67 and P89. There were no hydrogen bonding, electrostatic, or 6−12 Lennard-Jones empirical potential energy terms in the target function.

The number of observed intermolecular NOEs (36) were insufficient for a detailed structural analysis of the $ZipA_{185-328}$ complex with the FtsZ peptide but were sufficient for validating the peptides binding site and for generating a low-resolution structure of the complex. The low-resolution structure of $ZipA_{185-328}$ bound to the C-terminal FtsZ peptide followed the exact procedure for the structure determination of free $ZipA_{185-328}$ where the only modification was the incorporation of the FtsZ peptide and the addition of the peptide constraints to the free $ZipA_{185-328}$ constraints. The only modification to the free $ZipA_{185-328}$ constraints used for the $ZipA_{185-328}$−FtsZ peptide complex structure calculation was the removal of the side-chain (χ_1) torsion constraint for M42, which was inconsistent with the $ZipA_{185-328}$−FtsZ peptide complex. A total of 100 structures were calculated for the $ZipA_{185-328}$ complex with the FtsZ peptide where a

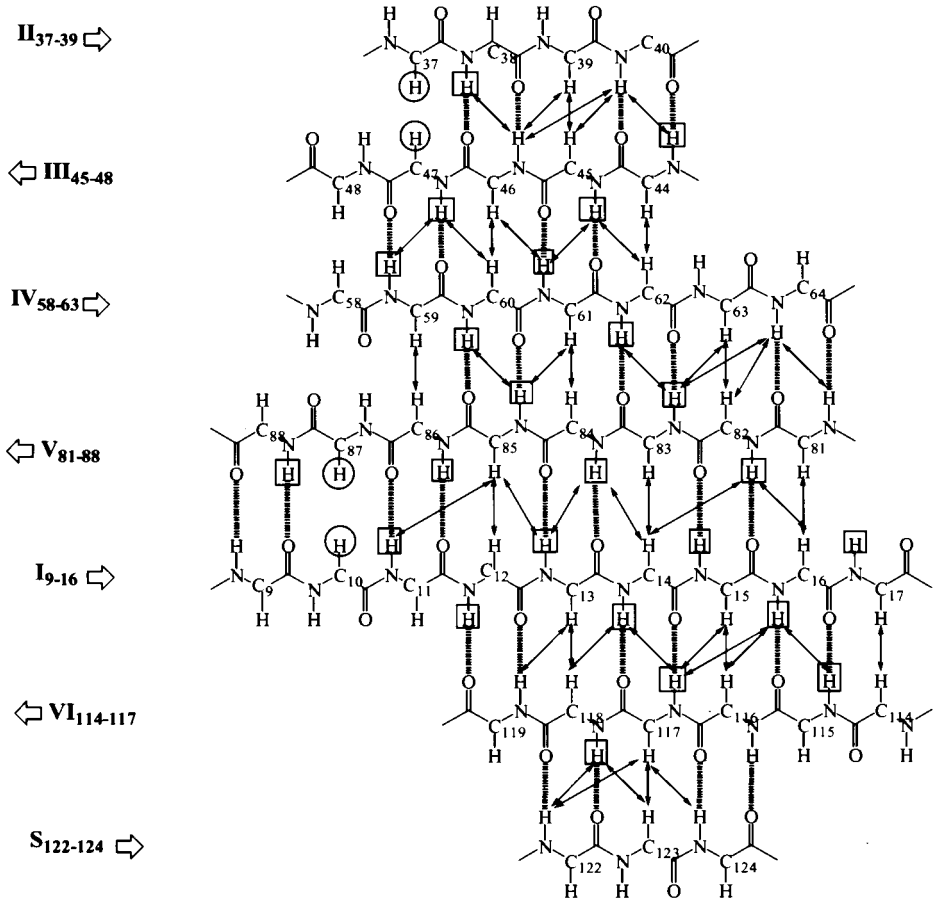

FIGURE 2: Secondary structure elements of ZipA as determined from qualitative analysis of the NOE and amide exchange data. β-strands are indicated on the left by roman numerals and the residue number range. Residues that are not defined as part of a β-strand but did exhibit preliminary data suggestive of a β-strand conformation are also illustrated. Particularly, residues 122−124 that do not conform to standard β-strand dihedral angles are labeled as S. Interstrand NOEs derived from the 3D ^{15}N- and ^{13}C-edited NOESY spectra are indicated by arrows, and slowly exchanging amide protons are boxed. Hydrogen bonds deduced from these data are shown as broken lines. Adjacent residues with degenerate Hα resonances are circled.

restrained minimized average structure was determined from the 30 best structures (Figure 5C).

Binding of C-terminal FtsZ Peptide with ZipA$_{185-328}$. Competition of the 17-amino acid peptide with FtsZ for binding to ZipA$_{185-328}$ was determined in an ELISA format. ZipA$_{185-328}$ was bound nonspecifically to the well of an Immulon 4HBX plate at 1μg ml^{-1}. After removing unbound ZipA$_{185-328}$ and blocking with BSA, the peptide (1−1000 μM) and FtsZ with an N-terminal FLAG epitope tag (2 μg ml^{-1}) were added to the wells for 2 h at room temperature. Unbound FtsZ was washed away, and the bound FtsZ was detected via FLAG monoclonal antibody and an anti-mouse IgG horseradish peroxidase conjugate. *o*-Phenylenediamine was used as a substrate for horseradish peroxidase, and after the reaction was stopped with diluted sulfuric acid the absorbance at 490 nm was read.

RESULTS

Secondary Structure Analysis. The regular secondary structure elements of ZipA$_{185-328}$ were identified from a qualitative analysis of sequential and interstrand NOEs, NH exchange rates, $^3J_{HN\alpha}$ coupling constants, and the ^{13}Cα and ^{13}Cβ secondary chemical shifts (*45*, *46*). The sequential and medium range NOEs were obtained from a qualitative analysis of the ^{15}N-edited NOESY and ^{13}C-edited NOESY spectra. $^3J_{HN\alpha}$ coupling constants were obtained from the relative intensity of Hα cross-peaks to the NH diagonal in the HNHA experiment (*15*). Slowly exchanging NH protons were identified by recording an HSQC spectra 1 day after exchanging a ZipA$_{185-328}$ sample from H_2O to D_2O. These data, together with the deduced secondary structure elements are summarized in Figure 1. On the basis of PROCHECK analysis, the overall structure of ZipA$_{185-328}$ is composed of three α-helices and a β-sheet consisting of six antiparallel β-strands (*47*, *48*). The three helical regions correspond to residues G25-Q34 (α_1); E94-V112 and (α_2) and P126-A144 (α_3); and the β-sheet region corresponds to residues A9-A16 (β_1), F37−F39 (β_2), Y45−H48 (β_3), L58-N63 (β_4), G81-V88 (β_5), and G114-L117 (β_6). The alignment of the β-sheet is illustrated in Figure 2. In addition, residues that exhibited NMR data suggestive of a β-strand conformation are also included in the figure.

Structure Determination. The final 30 simulated annealing structures were calculated on the basis of 2758 experimental NMR restraints consisting of 1954 approximate interproton distance restraints, 84 distance restraints for 42 backbone hydrogen bonds, 377 torsion angle restraints composed of 129 ϕ, 128 ψ, 92 χ1, and 28 χ2 torsion angle restraints, 113 $^3J_{NH\alpha}$ restraints, and 120 Cα and 110 Cβ chemical shift restraints. Stereospecific assignments were obtained for 63

Table 1: Structural Statistics and Atomic rms Differences[a]

Structural Statistics		
	⟨SA⟩	$(\overline{SA})_r$
rms deviations from experimental distance restraints (Å)[b]		
all (2038)	0.015 ± 0.002	0.013
interresidue sequential (|i − j| = 1) (637)	0.015 ± 0.004	0.011
interresidue short range (1 < |i − j| ≤ 5) (457)	0.012 ± 0.005	0.005
interresidue long-range (|i − j| > 5) (746)	0.018 ± 0.002	0.019
intraresidue (500)	0.005 ± 0.005	0.001
H-bonds (84)[c]	0.016 ± 0.004	0.020
rms deviation from exptl dihedral restraints (deg) (377)[b,d]	0.101 ± 0.058	0.130
rms deviation from exptl Cα restraints (ppm) (120)	0.97 ± 0.03	0.94
rms deviation from exptl Cβ restraints (ppm) (110)	0.87 ± 0.02	0.88
rms deviation from $^3J_{NH}\alpha$ restraints (Hz) (113)	0.60 ± 0.02	0.61
F_{NOE} (kcal mol^{-1})[e]	26.3 ± 7.2	19.7
F_{tor} (kcal mol^{-1})[e]	0.92 ± 0.67	0.39
F_{repel} (kcal mol^{-1})[e]	36.2 ± 3.4	19.1
F_{L-J} (kcal mol^{-1})[f]	−617 ± 8	−588
deviations from idealized covalent geometry		
bonds (Å) (2268)	0.003 ± 0	0.003
angles (deg) (4109)	0.485 ± 0.012	0.527
impropers (deg) (2163)[g]	0.432 ± 0.029	0.409
PROCHECK[h]		
overall G-factor	0.20 ± 0.001	0.12
% residues in most favorable region of Ramachandran plot	91.4 ± 1.4	91.1
H-bond energy	0.80 ± 0.04	0.80
no. of bad contacts/100 residues	6.9 ± 1.1	6.9

Atomic rms Differences (Å)

	residues 6−142		secondary structure[i]		ordered side chain[j]
	backbone atoms	all atoms	backbone atoms	all atoms	all atoms
⟨SA⟩ vs $\overline{SA}$	0.37 ± 0.04	0.78 ± 0.05	0.31 ± 0.04	0.72 ± 0.05	0.45 ± 0.04
⟨SA⟩ vs $(\overline{SA})_r$	0.41 ± 0.04	0.89 ± 0.05	0.35 ± 0.04	0.79 ± 0.06	0.51 ± 0.04
$(\overline{SA})_r$ vs $\overline{SA}$	0.16	0.43	0.14	0.39	0.23

[a] The notation of the structures is as follows: ⟨SA⟩ are the final 30 simulated annealing structures; $\overline{SA}$ is the mean structure obtained by averaging the coordinates of the individual SA structures best fit to each other (excluding residues 1−5 and 143−144); and $(\overline{SA})_r$ is the restrained minimized mean structure obtained by restrained minimization of the mean structure $\overline{SA}$ (*60*). The number of terms for the various restraints is given in parentheses. [b] None of the structures exhibited distance violations greater than 0.2 Å or dihedral angle violations greater than 1°. [c] For backbone NH−CO hydrogen bond there are two restraints: r_{NH-O} = 1.5−2.3 Å and r_{N-O} = 2.5−3.3 Å. All hydrogen bonds involve slowly exchanging NH protons. [d] The torsion angle restraints comprise 129 ϕ, 128 ψ, 92 χ1, and 28 χ2 restraints. [e] The values of the square-well NOE (F_{NOE}) and torsion angle (F_{tor}) potentials [cf. eqs 2 and 3 in Clore et al., (1986) (*32*)] are calculated with force constants of 50 kcal mol^{-1} Å^{-2} and 200 kcal mol^{-1} rad^{-2}, respectively. The value of the quartic van der Waals repulsion term (F_{repel}) [cf. eq 5 in Nilges et al. (1988) (*38*)] is calculated with a force constant of 4 kcal mol^{-1} Å^{-4} with the hard-sphere van der Waals radius set to 0.8 times the standard values used in the CHARMM (*61*) empirical energy function (*38*, *60*, *62*). [f] E_{L-J} is the Lennard−Jones−van der Waals energy calculated with the CHARMM emperical energy function and is *not* included in the target function for simulated annealing or restrained minimization. [g] The improper torsion restraints serve to maintain planarity and chirality. [h] These were calculated using the PROCHECK program (*48*). [i] The residues in the regular secondary structure are 25−34 (α_1), 94−112 (α_2), 126−144 (α_3), 9−16 (β_1), 37−39 (β_2), 45−48 (β_3), 58−63 (β_4), 81−88 (β_5), and 114−117 (β_6). [j] The disordered side chains that were excluded are as follows: residues 1−5; residues 143−144; Arg 6 from Cγ; Lys 7 from Cδ; Glu 8 from Cγ; His 18 beyond Cγ; His 19 from Cγ; Glu 22 beyond Cδ; Glu 26 beyond Cδ; Asn 30 from Cγ; Ser 31 beyond Cβ; Gln 33 from Cδ; Gln 34 beyond Cδ; Asp 41 beyond Cγ; Met 42 beyond Cγ; Asn 43 beyond Cγ; His 46 beyond Cγ; Arg 47 beyond Cϵ; Asp 52 from Cγ; Ser 54 beyond Cγ; Asn 63 beyond Cγ; Met 64 beyond Cγ; Val 65 beyond Cβ; Lys 66 from Cδ; Asp 71 beyond Cγ; Glu 73 from Cδ; Met 74 from Cγ; Lys 75 beyond Cϵ; Asp 76 beyond Cγ; Met 86 beyond Sδ; Gln 87 beyond Cδ; Asp 93 from Cγ; Glu 94 from Cδ; Gln 96 beyond Cδ; Asn 97 beyond Cγ; Lys 99 beyond Cϵ; Leu 100 beyond Cγ; Gln 103 beyond Cδ; Asp 110 beyond Cγ; Glu 111 beyond Cδ; Asp 118 beyond Cγ; Gln 120 beyond Cδ; Arg 121 beyond Cδ; Arg 122 beyond Cδ; Met 123 from Cϵ; Gln 127 beyond Cδ; Lys 128 beyond Cϵ; Arg 130 from Cγ; Glu 131 from Cδ; Gln 133 beyond Cδ; Asp 134 beyond Cγ; Arg 137 beyond Cδ; Glu 138 from Cδ; Lys 140 beyond Cϵ; Asp 141 beyond Cγ.

of the 92 residues with β-methylene protons, for the methyl groups of 4 of the 9 Val residues, and for the methyl groups of 11 of the 12 Leu residues. In addition, all seven of the Phe residues and all three of the Tyr residues were well-defined, making it possible to assign NOE restraints to only one of the pair of the degenerate CδH and CϵH protons and to assign a χ_2 torsion angle restraint. A summary of the structural statistics for the final 30 simulated annealing (SA) structures of $ZipA_{185-328}$ is provided in Table 1, and a best fit superposition of the backbone atoms is shown in Figure 3. The atomic root mean square (rms) distribution of the 30 simulated annealing structures about the mean coordinate positions for residues 6−142 is 0.37 ± 0.04 Å for the backbone atoms, 0.78 ± 0.05 Å for all atoms, and 0.45 ± 0.04 Å for all atoms excluding disordered surface side chains (Table 1). The high quality of the $ZipA_{185-328}$ NMR structure is also evident by the results of the PROCHECK analysis where an overall G-factor of 0.12, a hydrogen bond energy of 0.80, and only 6.9 bad contacts/100 residues are consistent with a good quality structure comparable to ∼1 Å X-ray structure (*48*). Additionally, most of the backbone torsion angles for nonglycine residues lie within expected regions

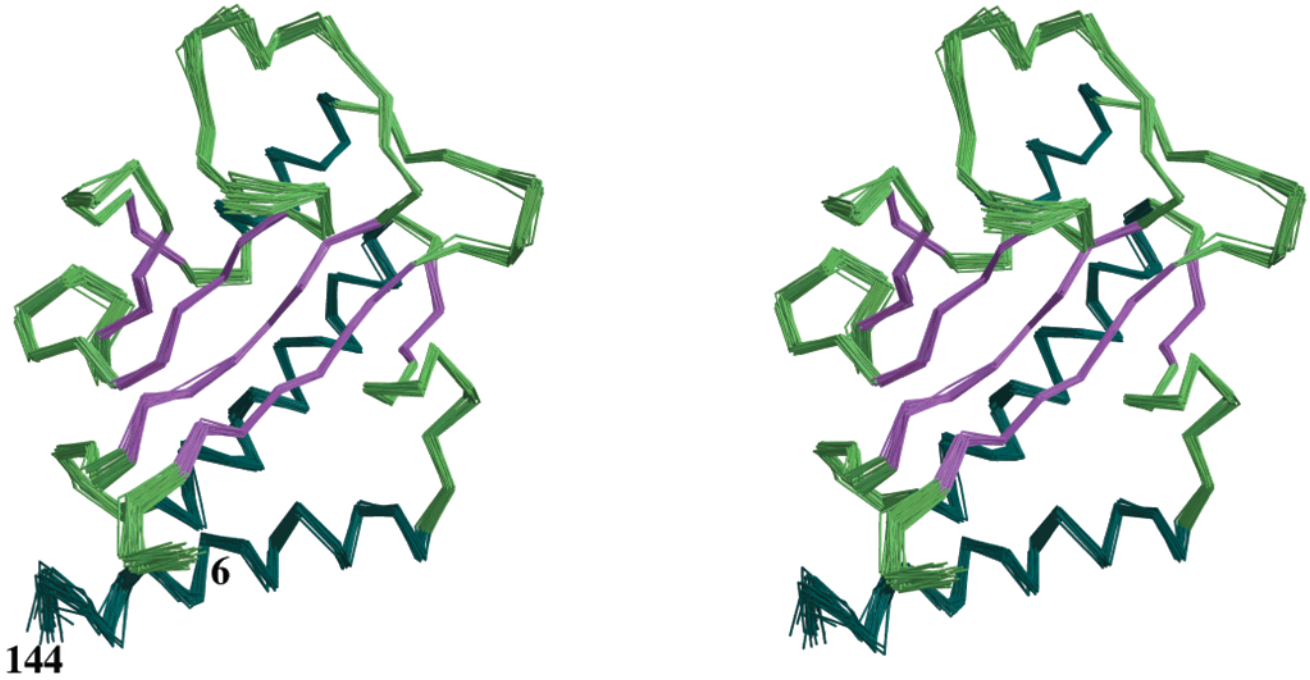

FIGURE 3: Stereoview of the backbone (N,C_α,C') superposition of the 30 best structures determined for $ZipA_{185-328}$ for residues 6−144 colored by secondary structure.

of the Ramachandran plot where 91.1% of the residues lie within the most favored region of the Ramachandran ϕ, ψ plot and 8.9% lie in the additionally allowed region.

DISCUSSION

$ZipA_{185-328}$ NMR Structure. The $ZipA_{185-328}$ protein adopts an α−β fold composed of three α-helices and a β-sheet consisting of six antiparallel β-strands (Figure 4). The previously reported NMR assignments and secondary structure determination for $ZipA_{185-328}$ (*8*) identified residues R122−M124 as a seventh β-strand based on observable interstrand NOEs and amide exchange rates (Figures 1 and 2), but the conformation of these residues in the solution structure of $ZipA_{185-328}$ reported herein do not conform with the definition of a β-sheet region based on standard ϕ and ψ torsion angles. Therefore, the overall topology for $ZipA_{185-328}$ is βαββββαβα where the β-sheet and α-helices form distinct surfaces directly opposite each other. The short β-strand (β_2) and residues R122−M124 are located at both edges of the β-sheet and directly follow β_I and $\beta_{III'}$ type turns, respectively. The β-strand (β_2) and residues R122−M124 effectively enter and exit the β-sheet where α_1 precedes β_2 and α_3 follows residues R122−M124. Thus, the short β-strand (β_2) and residues R122−M124 occur at the transition point between the β-sheet surface and the α-helical surface. In fact, the β-sheet as a whole does not form a perfectly flat surface, there is an effective twist perpendicular to the axis in the plane of the β-strands allowing for the transition from the β-sheet surface to the α-helical surface. This twist is most pronounced for β-strand β_2 and accounts for residues R122−M124 not conforming to a standard β-strand conformation. Another feature of the $ZipA_{185-328}$ structure is the loops between strands β_4 and β_5 and between strand β_1 and helix α_1. These loops come in close contact to nearly form a short β-sheet. A short helical region also occurs in the loop between β_4 and β_5. The combination of the potentially short β-sheet and helical region results in these two loops being relatively well-defined. Dynamic analysis of the $ZipA_{185-328}$ protein based on NH T1, T2, and NOE data indicates that the protein exhibits very little flexibility, even within loop regions, as evident by order-parameters (S^2) > 0.6 (data not shown) for all residues excluding the N- and C-terminus.

An additional feature of the $ZipA_{185-328}$ fold is the observation that all of the major loops of the structure effectively protrude from the surface composed of the β-sheet. This has the resulting effect of creating "channels" on the $ZipA_{185-328}$ surface (Figure 5A). This is significantly different from the surface created by the three α-helices, which does not have any distinguishing features (Figure 5B). An electrostatic surface potential for $ZipA_{185-328}$ indicates two distinct clusters within the observed "channels" on the β-sheet surface. These clusters correspond to a negative potential patch composed primarily of D118, D119, and E131 and a large hydrophobic patch comprised of residues V10, I12, A16, F39, M42, I44, A57, A62, M64, V65, P67, P80, and F85. The structure of the β-sheet surface is suggestive of a potential binding site for the interaction of $ZipA_{185-328}$ with FtsZ.

ZipA−FtsZ Interaction. A critical stage in *E. coli* cell division is the recruitment of ZipA to the FtsZ ring at the division site. It has been previously demonstrated that the recruitment of ZipA occurs through a direct binding interaction of ZipA with FtsZ (*4*). Furthermore, it has been determined that the FtsZ binding site within the ZipA structure occurs in the C-terminal domain (*6*). The *E. coli* FtsZ structure is composed of a large 320-amino acid N-terminal domain that is sufficient for FtsZ self-assembly and a small, variable in length C-terminal domain (*49*). Similar to ZipA, the binding site on *E. coli* FtsZ for ZipA

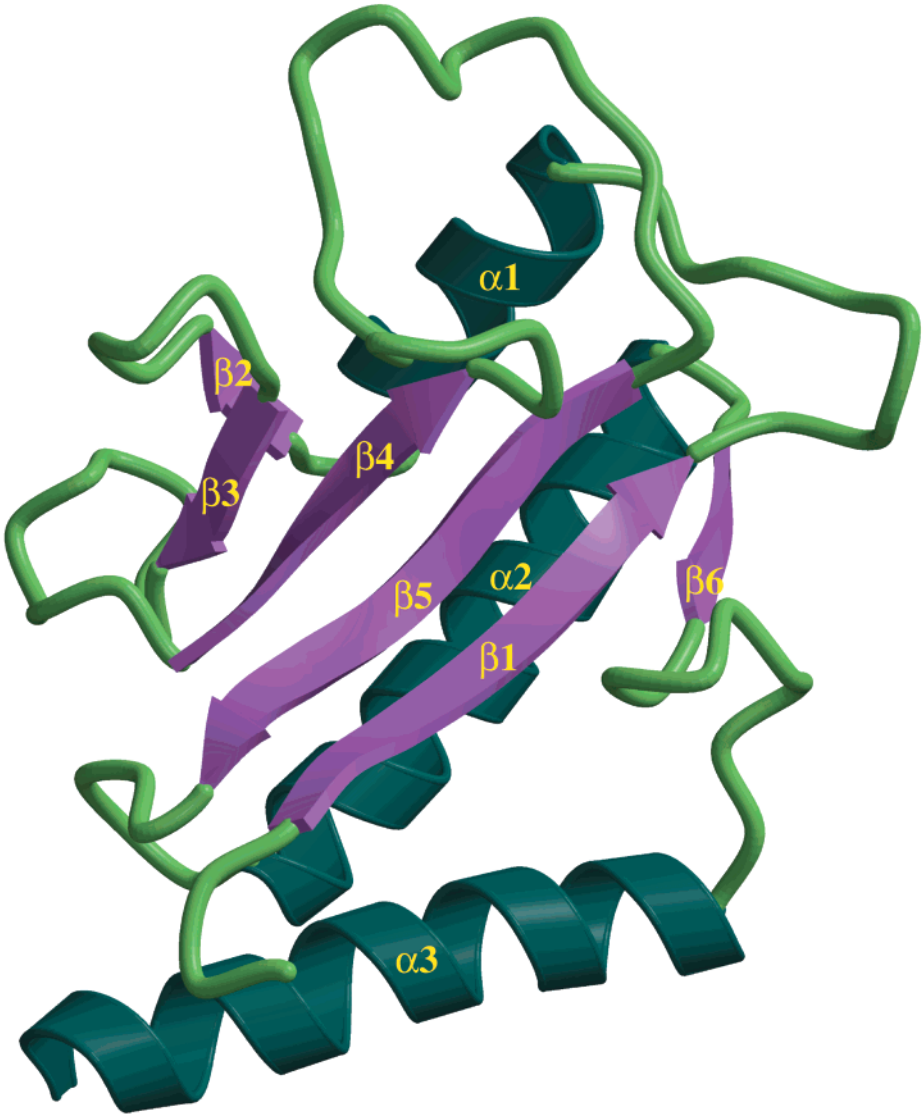

FIGURE 4: Ribbon diagram of the NMR structure of $ZipA_{185-328}$ for residues 6−144 colored by secondary structure. Secondary structure elements are labeled (same view as Figure 3).

has been identified as part of the 63-amino acid C-terminal region of the protein (*6*). Residues important for the interaction with ZipA have been further localized to the final 17 amino acids of the FtsZ C-terminus (S. Haney, personal communication). Examining the ZipA−FtsZ interaction with a yeast two-hybrid system, it was determined that a D373G mutation within FtsZ abrogated binding to ZipA, but could be suppressed by other mutations in the FtsZ C-terminus. While an X-ray structure of *Methanococcus jannischii* FtsZ has been solved, the structure lacks the C-terminal region identified to bind ZipA (*50*, *51*). As a result, there is a lack of structural information pertaining to the interaction of ZipA with FtsZ. The NMR solution structure described herein provides some insight into the nature of the interaction of ZipA with FtsZ since the details of the $ZipA_{185-328}$ surface suggests a potential FtsZ binding site among the observed "channels" within the β-sheet surface. These results along with the identification that the ZipA binding site in FtsZ is located in the C-terminal 17 amino acids led us to explore peptides from FtsZ for the ability to bind $ZipA_{185-328}$ and disrupt the binding of $ZipA_{185-328}$ with FtsZ.

To examine this possibility, a peptide encompassing the last 17 amino acids of *E. coli* FtsZ (^{367}KEPDYLDIPAFLRKQAD^{383}) was synthesized. Competition experiments (Figure 6A) demonstrate that this sequence is sufficient to inhibit binding of FtsZ to $ZipA_{23-328}$. As a control, a peptide incorporating the D373G mutation (using the numbering of the full-length protein) was also tested and showed an approximately 60-fold decrease in inhibition (Figure 6A). The same mutation in the full-length FtsZ results in a greater than 100-fold increase in the apparent dissociation constant (E. Glasfeld, unpublished results).

The 17-amino acid peptide from the C-terminus of *E. coli* FtsZ was found to directly bind $ZipA_{185-328}$ from chemical shift perturbations observed in a 2D ^{1}H-^{15}N HSQC spectra (Figure 6B). It is readily apparent from the 2D ^{1}H-^{15}N HSQC spectra that a considerable number of $ZipA_{185-328}$ residues are perturbed by the presence of the FtsZ C-terminal peptide. The residues that were significantly perturbed and readily assigned are mapped onto the $ZipA_{185-328}$ surface (Figure 5C). All of the residues that experience chemical shift changes in the presence of the FtsZ C-terminal peptide occur

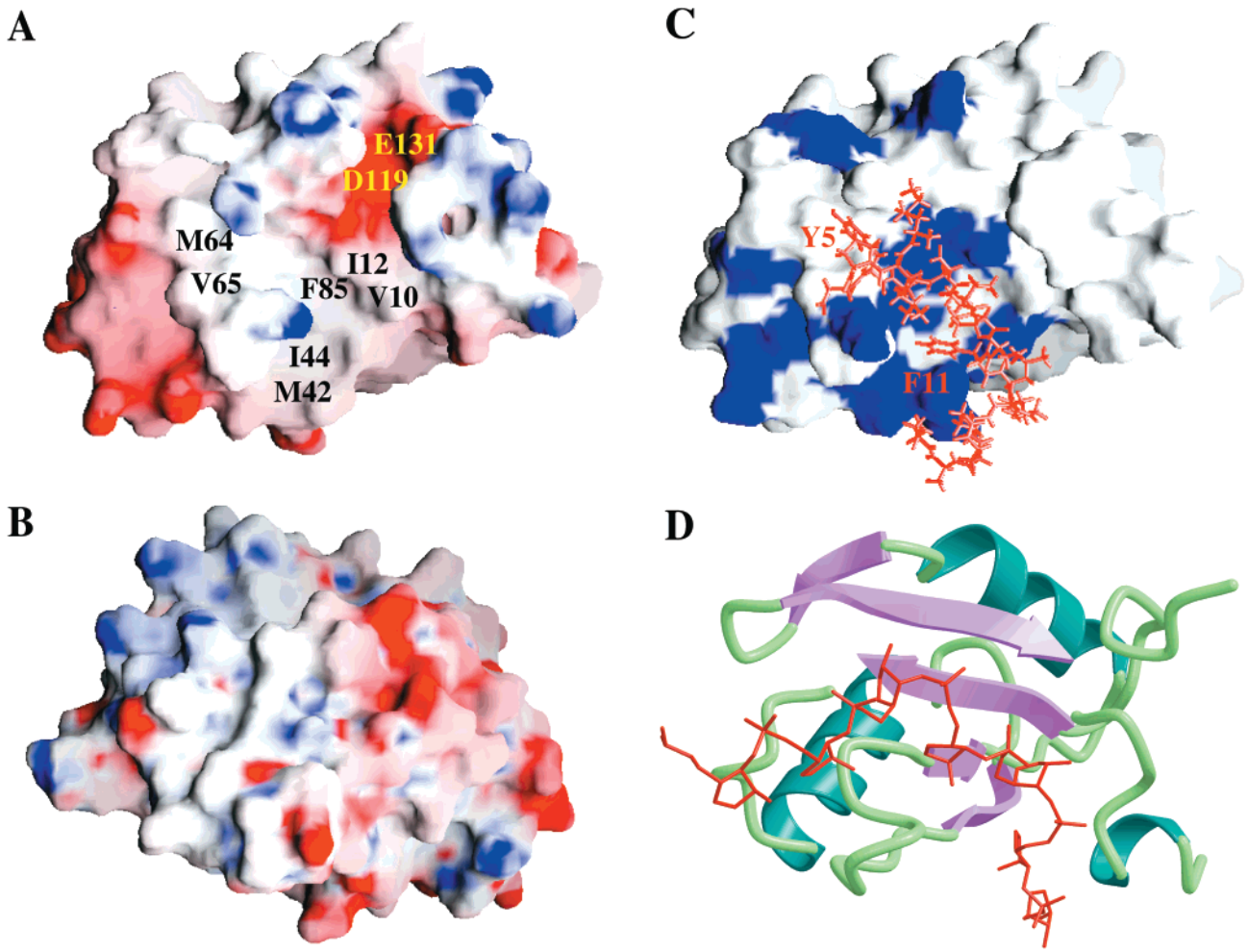

FIGURE 5: Molecular surface of the ZipA$_{185-328}$ NMR structure showing two different views: (A) ZipA$_{185-328}$ surface determined by the six-stranded β-sheet (same view as Figures 3 and 4) and (B) ZipA$_{185-328}$ surface determined by the three α-helices. Surfaces are colored according to electrostatic potential where red corresponds to negative, blue corresponds to positive, and white corresponds to neutral. Some key residues corresponding to different electrostatic potential regions and/or involved in the interaction with the FtsZ C-terminal peptide are labeled. (C) Molecular surface for ZipA$_{185-328}$ complexed with the FtsZ C-terminal peptide. Residues Y5 and F11 from the peptide are labeled. Same view as panel A, where residues exhibiting chemical shift perturbation in the presence of the FtsZ C-terminal peptide are colored blue (Figure 4B). Approximate positioning of the FtsZ C-terminal peptide (red) based on the nominal number of intermolecular NOEs is shown. (D) Ribbon diagram of the X-ray structure of the U1A spliceosomal protein complexed with an RNA hairpin (red) where only residues 6−11 for the RNA are shown (*52*). The U1A structure is aligned with the ZipA$_{185-328}$ NMR structure with the same view as panels A and C.

on the β-sheet surface in the vicinity of the observed "channels". The majority of these residues are located in β-strands β_1, β_2, β_4, and β_5 and the loops between β-strands $\beta_1-\beta_2$ and $\beta_4-\beta_5$. These results support the identification of the β-sheet as the primary FtsZ binding site on ZipA$_{185-328}$.

The interaction of the FtsZ C-terminal peptide with ZipA$_{185-328}$ was further confirmed by the observation of intermolecular NOEs between the FtsZ C-terminal peptide and ZipA$_{185-328}$ from the 3D ^{13}C-edited/^{12}C-filtered NOESY experiment. The FtsZ C-terminal peptide binds relatively weakly to ZipA$_{185-328}$ with an observed K_d of ~20 μM, but a total of 36 intermolecular NOEs were observed. The relatively weak affinity of the FtsZ peptide with ZipA$_{185-328}$ complicated the assignment and analysis of the complex data. Briefly, under conditions where the FtsZ peptide was in excess relative to ZipA$_{185-328}$, the 2D-filtered experiments yielded spectra consistent with the free FtsZ C-terminal peptide. Conversely, 2D-filtered experiments collected with an equimolar sample of ZipA$_{185-328}$ with FtsZ C-terminal peptide had a significant reduction in signal-to-noise displaying primarily intraresidue and sequential NOEs. This resulted in a complete lack of observable structurally significant intramolecular NOEs for the peptide in the complex. Additionally, the assignments of the peptide in the complex primarily relied on direct comparison of the spectra of the complex with the free peptide. Nevertheless, the assignments for Y5 and F11 were unambiguous because of the strong NOEs and distinct chemical shifts of the aromatic side chains. Coincidentally, the NOEs from the 3D ^{13}C-edited/^{12}C-filtered NOESY experiment were primarily between the peptide aromatic side chains of Y5 and F11 to two distinct regions of ZipA. In particular, Y5 from the peptide exhibited NOEs to ZipA$_{185-328}$ residues M64, V65, and R121, and F11 from the peptide showed NOEs to ZipA$_{185-328}$ residues M42, I44, A62, G68, and T69. The ZipA$_{185-328}$−peptide structure indicates that the peptide binds within the hydrophobic channel on the β-sheet surface of ZipA$_{185-328}$ consistent with the previously described 2D ^{1}H-^{15}N HSQC chemical shift perturbations (Figure 6B). It is important to note that chemical shifts are very sensitive to changes in the local

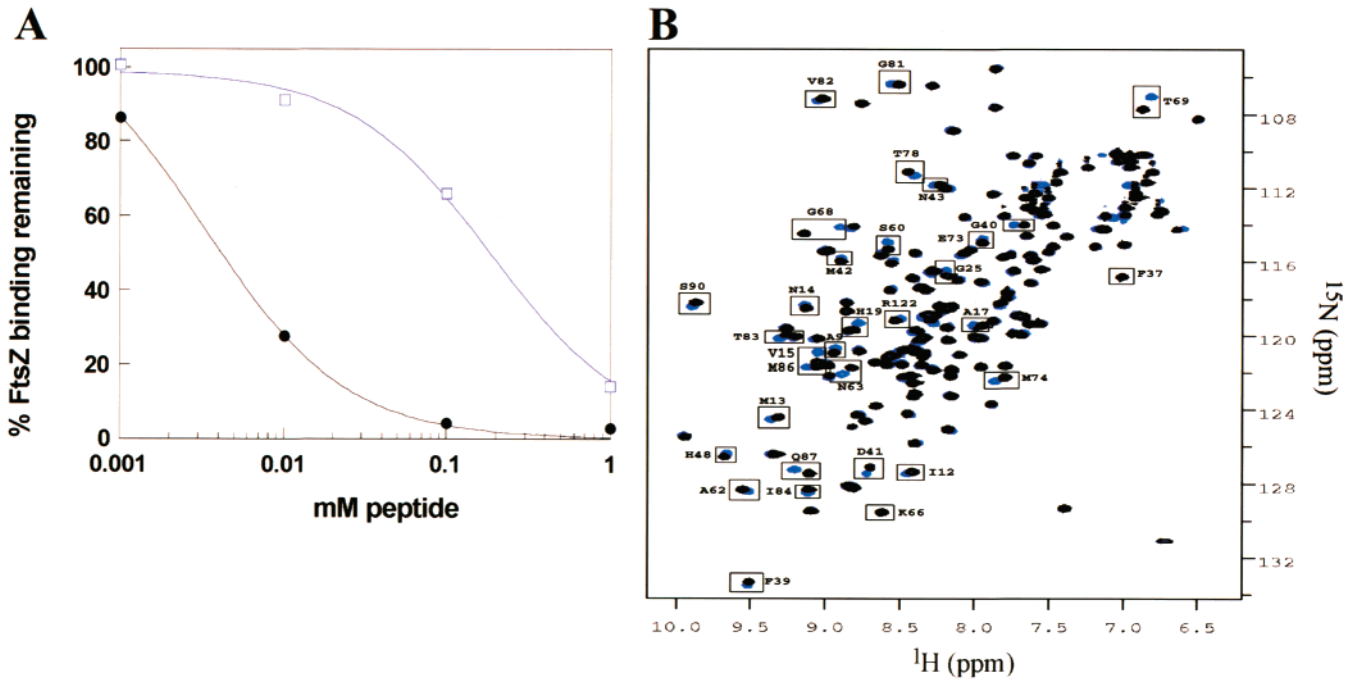

FIGURE 6: (A) Titration data demonstrating the relative inhibition of the ZipA$_{23-328}$−FtsZ interaction by the peptides (●) KEPDYLDIPAFLRKQAD and (□) KEPDYLGIPAFLRKQAD. (B) Overlay of the ^{1}H-^{15}N spectra for free ZipA$_{185-328}$ (black) and ZipA$_{185-328}$ complexed with the C-terminal peptide (blue), KEPDYLDIPAFLRKQAD. Residues exhibiting significant chemical shift perturbation are boxed and labeled.

environment and a perturbation may arise from either a direct interaction with the peptide or from an induced conformational change due to the presence of the peptide.

On the basis of the nominal number of intermolecular NOEs, only a low-resolution structure of the complex was attainable (Figure 5C). Given the minimal experimental information for the ZipA$_{185-328}$−peptide complex, it is best to view the complex structure as an approach to further define the FtsZ C-terminal peptide binding-site relative to the chemical shift perturbation data. The low-resolution structure of the ZipA$_{185-328}$−peptide complex was calculated using the constraints for free ZipA$_{185-328}$ appended with the 36 intermolecular NOEs between ZipA$_{185-328}$ and the FtsZ C-terminal peptide using the identical approach as the free ZipA$_{185-328}$ structure calculation. Interestingly, except for excluding the side chain χ_2 constraint for M42, no significant constraint violations were observed for the ZipA$_{185-328}$ structure in the complex, suggesting a minimal perturbation in the overall ZipA$_{185-328}$ structure in the presence of the peptide. This result provides validation for the use of the free ZipA$_{185-328}$ constraints to expedite the complex structure calculation. The structure of the ZipA$_{185-328}$−peptide complex indicates the general binding location and orientation of the peptide binding to ZipA$_{185-328}$ but infers very little information on the structure of the peptide or perturbation in the ZipA$_{185-328}$ structure and minimal information of the interaction of ZipA$_{185-328}$ with the FtsZ C-terminal peptide. Effectively, the available experimental data approximately positions the side chains for Y5, L6, I8, and F11, but the remainder of the residues from the FtsZ C-terminal peptide do not exhibit any observable intermolecular NOEs. Thus, the positioning of these remaining residues is predominately determined by constraints imposed from the binding of Y5, L6, I8, and F11 and from positive interactions with ZipA$_{185-328}$ based on standard modeling force field energies. Nevertheless, the combination of the chemical shift perturbation data and the intermolecular NOEs effectively define the FtsZ C-terminal peptide binding site on ZipA$_{185-328}$ while identifying key residues from ZipA$_{185-328}$ that are potentially involved in binding FtsZ.

Similarity Between ZipA Fold and RNA-Binding Motif. The observed fold for ZipA$_{185-328}$ has similarities to the split $\beta-\alpha-\beta$ fold observed in many RNA-binding proteins containing the ribonucleoprotein sequence motif (RNP). The split $\beta-\alpha-\beta$ fold is described as an α/β sandwich composed of a four-stranded anitparallel β-sheet packed against two α-helices (*52*−*58*). As expected, despite this apparent structural homology, there is no observable sequence similarity between ZipA$_{185-328}$ and the RNP sequence motif. Also, the ZipA$_{185-328}$ fold has additional features not present in the RNP sequence motif. Particularly, ZipA$_{185-328}$ contains a third α-helix where the three helices pack closer to parallel relative to the approximate perpendicular packing in the RNP domain. The helices are generally longer in the ZipA$_{185-328}$ structure: 9−18 residues for ZipA$_{185-328}$ as compared with 10−11 residues for the RNP domain. Similarly, the β-sheet is larger and composed of six β-strands in ZipA$_{185-328}$ as compared to four strands in the RNP domain.

The RNP domain is a very common eukaryotic protein domain that is involved in the recognition of a wide range of RNA structures. The crystal structure of U1A spliceosomal protein complexed with a 21-residue snRNA hairpin turn indicates that the interaction between U1A and the RNA molecule occurs exclusively in the β-sheet (*52*). A significant component of the binding is a hydrophobic interaction between the RNA bases and two highly conserved U1A aromatic residues (*59*). Furthermore, the U1A loop 3 plays a crucial role in defining the surface geometry of the binding interface. These features are very reminiscent of the FtsZ binding site on ZipA$_{185-328}$ identified from the ZipA$_{185-328}$

NMR structure, the 2D ^{1}H-^{15}N HSQC chemical shift perturbations, and the intermolecular NOEs. A ribbon diagram of the U1A X-ray structure complexed with the RNA hairpin is illustrated in Figure 5D. The U1A X-ray structure was aligned with the $ZipA_{185-328}$ NMR structure based on the common secondary structure elements. Superposition of the Cα atoms between the four β-strands of the U1A X-ray structure with comparable β-strands from the $ZipA_{185-328}$ NMR structure (β_1, β_4, β_5, and β_6) results in an rms difference of 2.70 Å. Including the α-helices from U1A spliceosomal protein in the alignment with $ZipA_{185-328}$ (α_1 and α_2) increases the resulting rms to 3.94 Å. This comparison implies that the structural similarity between $ZipA_{185-328}$ and U1A spliceosomal protein is primarily limited to the overall folding motif.

It is readily apparent from Figure 5, panels B and D that the U1A RNA binding site correlates very well with the observed chemical shift perturbations observed for $ZipA_{185-328}$ in the presence of the FtsZ C-terminal peptide. In fact, the relative positioning of the FtsZ C-terminal peptide in the ZipA binding site correlates equally well with the binding of the RNA hairpin in U1A (Figure 5, panels C and D). The striking correlation between the U1A RNA binding site and the proposed $ZipA_{185-328}$ FtsZ C-terminal peptide binding site in addition to the similarity between the protein folds may provide further insight into the ZipA−FtsZ interaction. It is plausible that characteristics of the ZipA−FtsZ binding interaction may be consistent with the observed features of the U1A−RNA complex, especially given that the major interactions observed between $ZipA_{185-328}$ and the FtsZ C-terminal peptide are mediated by Y5 and F11 consistent with the hydrophobic nature of the U1A−RNA interaction. Additionally, the observation that a structural motif is adaptable to function as either an RNA- or protein-binding domain is an intriguing consequence of the determination of the $ZipA_{185-328}$ NMR structure. The observed fold for the $ZipA_{185-328}$ protein in conjunction with the identification of the potential FtsZ binding site is an important step toward understanding the details of the ZipA−FtsZ interaction and establishing a structure-based approach to designing inhibitors of the ZipA−FtsZ complex.

REFERENCES

1. Bramhill, D. (1997) *Annu. Rev. Cell Dev. Biol. 13*, 395−424.
2. Lutkenhaus, J., and Addinall, S. G. (1997) *Annu. Rev. Biochem. 66*, 93−116.
3. Rothfield, L. I., and Justice, S. S. (1997) *Cell 88*, 581−584.
4. Hale, C. A., and de Boer, P. A. J. (1997) *Cell 88*, 175−185.
5. Hale, C. A., and De Boer, P. A. J. (1999) *J. Bacteriol. 181*, 167−176.
6. Liu, Z., Mukherjee, A., and Lutkenhaus, J. (1999) *Mol. Microbiol. 31*, 1853−1861.
7. RayChaudhuri, D. (1999) *EMBO J. 18*, 2372−2383.
8. Moy, F. J., Glasfeld, E., and Powers, R. (2000) *J. Biomol. NMR*, submitted for publication.
9. Piotto, M., Saudek, V., and Sklenar, V. (1992) *J. Biomol. NMR 2*, 661−665.
10. Grzesiek, S., and Bax, A. (1993) *J. Am. Chem. Soc. 115*, 12593−12594.
11. Marion, D., Ikura, M., Tschudin, R., and Bax, A. (1989) *J. Magn. Reson. 85*, 393−399.
12. Delaglio, F., Grzesiek, S., Vuister, G. W., Zhu, G., Pfeifer, J., and Bax, A. (1995) *J. Biomol. NMR 6*, 277−293.
13. Garrett, D. S., Powers, R., Gronenborn, A. M., and Clore, G. M. (1991) *J. Magn. Reson. 95*, 214−220.
14. Zhu, G., and Bax, A. (1992) *J. Magn. Reson. 100*, 202−207.
15. Vuister, G. W., and Bax, A. (1993) *J. Am. Chem. Soc. 115*, 7772−7777.
16. Archer, S. J., Ikura, M., Torchia, D. A., and Bax, A. (1991) *J. Magn. Reson. 95*, 636−641.
17. Grzesiek, S., Kuboniwa, H., Hinck, A. P., and Bax, A. (1995) *J. Am. Chem. Soc. 117*, 5312−5315.
18. Marion, D., Driscoll, P. C., Kay, L. E., Wingfield, P. T., Bax, A., Gronenborn, A. M., and Clore, G. M. (1989) *Biochemistry 28*, 6150−6156.
19. Zuiderweg, E. R. P., and Fesik, S. W. (1989) *Biochemistry 28*, 2387−2391.
20. Zuiderweg, E. R. P., McIntosh, L. P., Dahlquist, F. W., and Fesik, S. W. (1990) *J. Magn. Reson. 86*, 210−216.
21. Ikura, M., Kay, L. E., Tschudin, R., and Bax, A. (1990) *J. Magn. Reson. 86*, 204−209.
22. Grzesiek, S., and Bax, A. (1992) *J. Am. Chem. Soc. 114*, 6291−6293.
23. Grzesiek, S., Anglister, J., and Bax, A. (1993) *J. Magn. Reson., Ser. B 101*, 114−119.
24. Moy, F. J., Chanda, P., K., Chen, J., M., Cosmi, S., Edris, W., Skotnicki, J. S., Wilhelm, J., and Powers, R. (1999) *Biochemistry 38*, 7085−7096.
25. Jeener, J., Meier, B. H., Bachmann, and Ernst, R. R. (1979) *J. Chem. Phys. 71*, 4546−4553.
26. Bax, A., and Davis, D. G. (1985) *J. Magn. Reson. 65*, 355−360.
27. Trimble, L. A., and Bernstein, M. A. (1994) *J. Magn. Reson., Ser. B 105*, 67−72.
28. Wuthrich, K. (1986) *NMR of Proteins and Nucleic Acids*, John Wiley & Sons, Inc., New York.
29. Ikura, M., and Bax, A. (1992) *J. Am. Chem. Soc. 114*, 2433−2440.
30. Lee, W., Revington, M. J., Arrowsmith, C., and Kay, L. E. (1994) *FEBS Lett. 350*, 87−90.
31. Williamson, M. P., Havel, T. F., and Wuethrich, K. (1985) *J. Mol. Biol. 182*, 295−315.
32. Clore, G. M., Nilges, M., Sukumaran, D. K., Bruenger, A. T., Karplus, M., and Gronenborn, A. M. (1986) *EMBO J. 5*, 2729−2735.
33. Wuthrich, K., Billeter, M., and Braun, W. (1983) *J. Mol. Biol. 169*, 949−961.
34. Zuiderweg, E. R. P., Boelens, R., and Kaptein, R. (1985) *Biopolymers 24*, 601−611.
35. Bax, A., and Pochapsky, S. S. (1992) *J. Magn. Reson. 99*, 638−643.
36. Powers, R., Garrett, D. S., March, C. J., Frieden, E. A., Gronenborn, A. M., and Clore, G. M. (1993) *Biochemistry 32*, 6744−6762.
37. Cornilescu, G., Delaglio, F., and Bax, A. (1999) *J. Biomol. NMR 13*, 289−302.
38. Nilges, M., Gronenborn, A. M., Bruenger, A. T., and Clore, G. M. (1988) *Protein Eng. 2*, 27−38.
39. Clore, G. M., Appella, E., Yamada, M., Matsushima, K., and Gronenborn, A. M. (1990) *Biochemistry 29*, 1689−1696.
40. Brunger, A. T. (1993) *X-PLOR*, Version 3.1 Manual, Yale University, New Haven, CT.
41. Garrett, D. S., Kuszewski, J., Hancock, T. J., Lodi, P. J., Vuister, G. W., Gronenborn, A. M., and Clore, G. M. (1994) *J. Magn. Reson., Ser. B 104*, 99−103.
42. Kuszewski, J., Qin, J., Gronenborn, A. M., and Clore, G. M. (1995) *J. Magn. Reson., Ser. B 106*, 92−96.
43. Kuszewski, J., Gronenborn, A. M., and Clore, G. M. (1996) *Protein Sci. 5*, 1067−1080.
44. Kuszewski, J., Gronenborn, A. M., and Clore, G. M. (1997) *J. Magn. Reson. 125*, 171−177.
45. Clore, G. M., and Gronenborn, A. M. (1989) *Crit. Rev. Biochem. Mol. Biol. 24*, 479−564.
46. Wishart, D. S., and Sykes, B. D. (1994) *Methods Enzymol. 239*.
47. Laskowski, R. A., MacArthur, M. W., Moss, D. S., and Thornton, J. M. (1993) *J. Appl. Crystallogr. 26*, 283−291.

48. Laskowski, R., Rullmannn, J., MacArthur, M., Kaptein, R., and JM, T. (1996) *J. Biomol. NMR 8*, 477−486.
49. Wang, X., Huang, J., Mukherjee, A., Cao, C., and Lutkenhaus, J. (1997) *J. Bacteriol. 179*, 5551−5559.
50. Lowe, J. (1998) *J. Struct. Biol. 124*, 235−243.
51. Lowe, J., and Amos, L. A. (1998) *Nature 391*, 203−206.
52. Oubridge, C., Ito, N., Evans, P. R., Teo, C. H., and Nagai, K. (1994) *Nature 372*, 432−438.
53. Lu, J., and Hall, K. B. (1997) *Biochemistry 36*, 10393−10405.
54. Nagai, K., Oubridge, C., Jessen, T. H., Li, J., and Evans, P. R. (1990) *Nature 348*, 515−520.
55. Avis, J. M., Allain, F. H. T., Howe, P. W. A., Varani, G., Nagai, K., and Neuhaus, D. (1996) *J. Mol. Biol. 257*, 398−411.
56. Wittekind, M., Gorlach, M., Friedrichs, M., Dreyfuss, G., and Mueller, L. (1992) *Biochemistry 31*, 6254−6265.
57. Lee, A. L., Kanaar, R., Rio, D. C., and Wemmer, D. E. (1994) *Biochemistry 33*, 13775−13786.
58. Garrett, D. S., Lodi, P. J., Shamoo, Y., Williams, K. R., Clore, G. M., and Gronenborn, A. M. (1994) *Biochemistry 33*, 2852−2858.
59. Allain, F. H. T., Howe, P. W. A., Neuhaus, D., and Varani, G. (1997) *EMBO J. 16*, 5764−5774.
60. Nilges, M., Clore, G. M., and Gronenborn, A. M. (1988) *FEBS Lett. 239*, 129−136.
61. Brooks, B. R., Bruccoleri, R. E., Olafson, B. D., States, D. J., Swaminathan, S., and Karplus, M. (1983) *J. Comput. Chem. 4*, 187−217.
62. Nilges, M., Clore, G. M., and Gronenborn, A. M. (1988) *FEBS Lett. 229*, 317−324.

BI0009690